Shielding Design for High-Frequency Wireless Power Transfer System for EV Charging With Self-Resonant Coils

Ruiyang Qin, *Student Member, IEEE*, Jie Li, *Student Member, IEEE*, Jingjing Sun, *Student Member, IEEE*, and Daniel Costinett, *Senior Member, IEEE*

***Abstract*—This article provides a complete coil and shielding design solution for a 6.6 kW electric vehicle (EV) wireless power transfer system based on compact self-resonant (SR) coils. Due to the presence of a conductive vehicle body above the receiver coil, vertical fringing flux must be shielded in any EV wireless charger. Using high-frequency SR coils, parasitic capacitance introduced by standard shielding design approaches degrades the quality factor of the coils. In this article, the high-frequency parasitic capacitance introduced by the magnetic and conductive shielding materials is analyzed in detail, and a shielding geometry optimization method is proposed. Using ferrite and an additional dielectric spacer, prototype aluminum-backed SR coils are fabricated to validate the modeling. The total thicknesses of the transmitter and receiver coils are only 11.4 and 7.4 mm, respectively. The prototype coils achieve 92.3% dc–dc efficiency and 7.1 kW/dm^3 volumetric power density. This article demonstrates the first 6.6 kW WPT system for EV charging using compact megahertz-SR coils including a complete magnetic and conductive shielding implementation.**

***Index Terms*—Electric vehicle (EV) charging, multilayer spiral coil, self-resonant (SR) coil, shielding design, wireless power transfer (WPT).**

I. Introduction

With the increasing interest in lightweight and compact wireless charging systems for electric vehicles (EV), high-frequency wireless power transfer (WPT) systems have drawn more attention nowadays. Multiple coil design approaches at MHz have been reported, using various self-resonant (SR) coil structures [1], [2], [3], [4], [5], [6] to achieve compact size and high quality factor. Without the need for external lumped capacitors for compensation, SR coils achieve high power density and greatly reduced capacitor thermal stress due to the distributed capacitance [7], [8].

However, when installed in an EV, any unshielded charging coils will exert high leakage magnetic field, causing excessive eddy current loss on the structural elements of the vehicle chassis like carbon steel or aluminum alloys. To avoid such high power loss on the chassis, and to attenuate stray field in surrounding areas, proper shielding is required for any coil, including SR coils, especially on the receiver side. To reduce the leakage magnetic field, different shielding approaches have been studied, mainly including conductive shielding [9], [10], magnetic shielding [11], and active shielding [12], [13], [14].

Conductive shielding utilizes an opposing magnetic field induced in a metal plate to counteract the vertical fringing field above the receiver coil. The conductive shield may also be used as a heatsink and to provide structural strength for the whole coil assembly. Different metal materials including copper and aluminum are compared in [9] to study the effectiveness of shielding. Instead of counteracting the fringing field, magnetic shielding using ferrite concentrates the flux around the coil, which reduces the leakage flux while increasing the coil coupling coefficient. A wing shape ferrite is used in [11] for better shielding performance.

Conductive shielding and magnetic shielding are often applied together. SAE J2954 contains standards for the typical size and dimension of shielding using metal plates and ferrite [15]. Active shielding approaches use additional reactive *LC* resonant coils around the main coil to cancel the fringing field [12], [13]. In [14], the phases of winding currents are controlled to minimize stray field. Still, additional components and a more complicated control algorithm are required for active shielding and may increase the cost and size of the system.

Prior work focuses on the study of shielding design for the WPT systems with Litz windings in a relatively low-frequency range below 100 kHz. No work reported so far discusses the shielding consideration for high-frequency WPT systems with SR coils for EV applications. Of all the SR coils in [1], [2], [3], [4], [5], [6], [7], [8], only the structures from [3] and [8] have demonstrated power delivery in excess of 1 kW and frequencies beyond 1 MHz for potential EV applications. As demonstrated in [16], [17], and [18], these designs reach much higher gravimetric

Manuscript received 1 July 2022; revised 19 October 2022 and 8 January 2023; accepted 18 February 2023. Date of publication 3 March 2023; date of current version 20 April 2023. This work was supported in part by II-VI Foundation Block-Gift Graduate Research Program, in part by Engineering Research Center Shared Facilities supported by the Engineering Research Center Program of the National Science Foundation, in part by the Department of Energy under NSF Award Number EEC-1041877, and in part by the CURENT Industry Partnership Program. Recommended for publication by Associate Editor A. Barrado. *(Corresponding author: Ruiyang Qin.)*

The authors are with the Min H. Kao Department of Electrical Engineering and Computer Science, University of Tennessee, Knoxville, TN 37996 USA (e-mail: ruiyangq@gmail.com; jli94@vols.utk.edu; jsun30@vols.utk.edu; daniel.costinett@utk.edu).

Color versions of one or more figures in this article are available at https://doi.org/10.1109/TPEL.2023.3251990.

Digital Object Identifier 10.1109/TPEL.2023.3251990

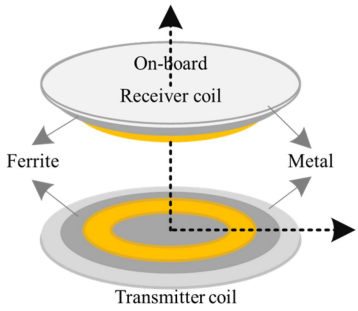

Fig. 1. Proposed shielding structure for WPT system with SR coils.

and volumetric power densities compared to other state-of-the-art WPT systems operating at frequencies below 100 kHz. The study in [19] explores the possibility of shielding MHz-range SR coils using a resonant reactive coil, but the shielding effect is limited.

In this article, a complete shielding design solution is provided based on the previously-reported 3 MHz multilayer non-uniform SR coils, shown in Fig. 1 [17]. With the existence of both ferrite and aluminum, the impact of shielding on the multi-layer SR coil at frequencies above 1 MHz is analyzed in detail. Design guidelines are provided for the ferrite geometries, and an integrated WPT system design optimization process is proposed. To verify the design result, a shielding structure is assembled based on the previously-reported multilayer nonuniform SR coils and tested up to 6.6 kW. This article validates the performance of high-frequency WPT system with SR coils considering practical shielding implementation as required for EV wireless charging.

The rest of this article is organized as follows. Section II investigates the ferrite and metal impacts on the multilayer SR coil using a fast two-dimensional (2-D) magnetic field simulator. Section III presents the design guidelines for shielding geometry, with a focus on the impact of parasitic capacitance introduced by metal and ferrite shielding materials in the MHz range. Section IV gives the systematic shielding geometry optimization process. Section V presents the complete fabrication process and test results of the high-frequency WPT system with shielded SR coils. Section VI concludes the article.

II. Shielding Requirement for Self-Resonant Coils in EV Applications

The structure of the proposed multilayer, nonuniform, series-resonant SR coil is shown in Fig. 2. Three layers of copper spiral traces are stacked vertically, with two equal-thickness layers of dielectric material sandwiched between them. The current flows from terminal A on the top layer to terminal B on the bottom layer, gradually transitioning through both dielectric layers in series.

The total current is distributed over three layers of copper, controlled by the varying interlayer capacitance generated by the non-uniform copper widths w_1, w_2, and w_3. Together with the inductance from the spiral coils, the three-layer coil works as a series L–C resonant network. The proposed SR coil has the advantages of high inductance and high quality factor,

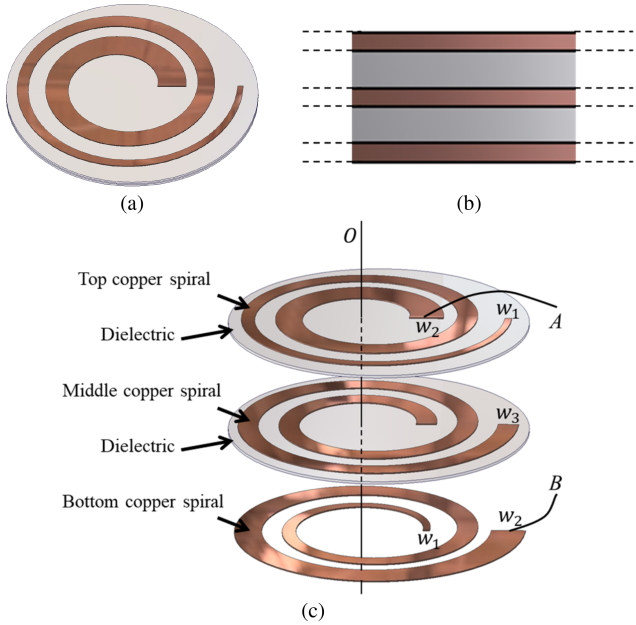

Fig. 2. Three-layer nonuniform SR coil structure (a) 3-D view (b) side view, and (c) exploded 3-D view [18].

providing a lightweight and low-cost solution for high power, high-frequency wireless EV charging [18].

A fast 2-D magnetic simulation is conducted in FEMM [20] first to illustrate the shielding challenge when the SR coils are deployed for EV charging. With the 2-D axisymmetric meshing setup shown in Fig. 3(a), (b), and (d) gives the magnetic field distribution for the 6.6 kW system with the proposed multi-layer SR coils. The coil radius is 200 mm with 17.9 A transmitter coil current, 11.9 A receiver coil current, 3.125 MHz frequency, and 100 mm airgap between two coils, following the design detailed in [18]. Significant fringing field exists above the top and below the bottom coils as shown in Fig. 3(b). These vertical fringing fields will induce eddy current loss in surrounding metal objects on the vehicle and destroy the coupling of coils.

One straightforward approach to shielding is to introduce conductive metal, as shown in Fig. 3(c). Identical 1 mm thick, 225 mm radius aluminum plates are placed 5 mm away from the coils. The magnetic field outside the plates is now constrained to just several microTesla. However, the opposing magnetic field generated by the eddy currents induced in the metal plate alters the field distribution around the coils. As a result, the coil inductance and coupling are greatly reduced, leading to a significant drop in coil-to-coil maximum efficiency as given in Table I .

In Fig. 3(d), ferrites are instead used to channel the flux around the coil. Most of the flux outside the two coils is now contained within the ferrite cores, with a boost in both inductance and coupling coefficient. Still, the leakage magnetic field above the receiver coil is much larger compared to the aluminum shielding case, with a much higher weight required for shielding.

Operation under misalignment may impact the shielding design, particularly the outer radius of the conductive shield. Because the magnetic fields of the coils are indistinguishable from

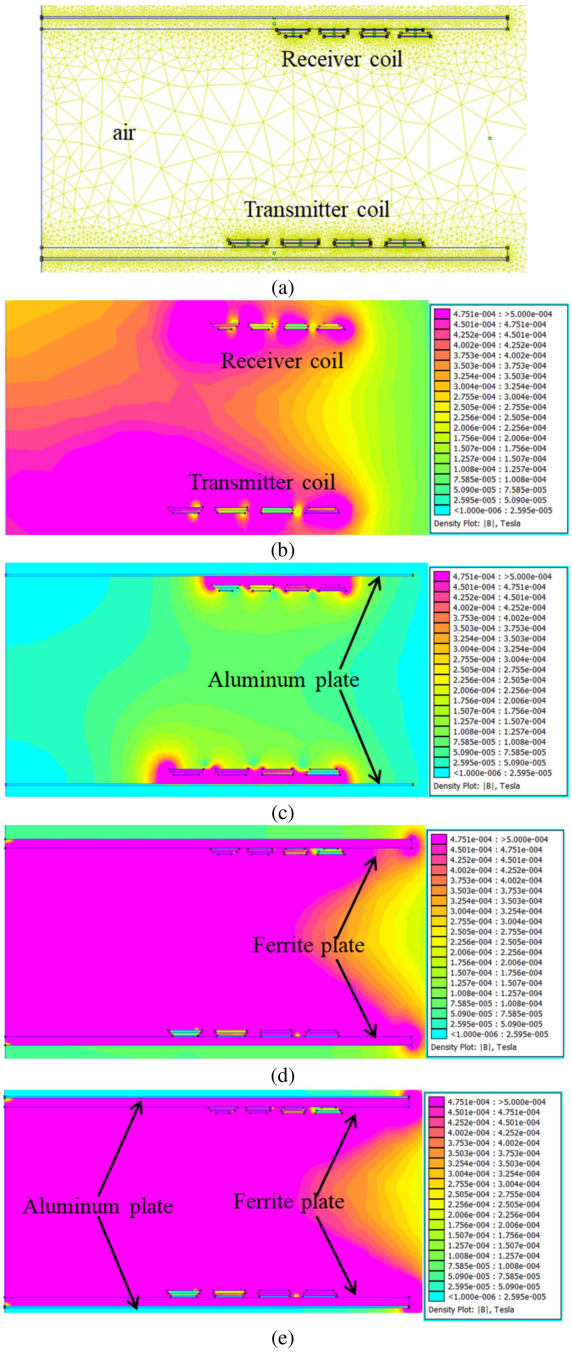

Fig. 3. FEMM-based 2-D magnetic field simulation for a 6.6 kW system with proposed multilayer SR coils. (a) Meshing setup in FEMM. (b) Magnetic field without shielding. (c) Magnetic field with aluminum shielding. (d) Magnetic field with ferrite shielding. (e) Magnetic field with ferrite + aluminum shielding.

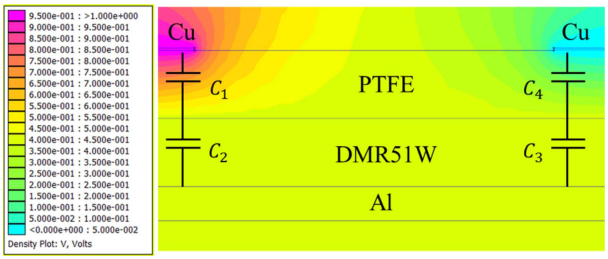

Fig. 4. FEMM based 2-D electric field simulation for the coil with shielding.

TABLE I
COIL INDUCTANCE AND COUPLING COMPARISON

Shielding method	Inductance [μH]		Quality factor @3MHz		Mutual inductance [μH]	Coupling coefficient
	TX	RX	TX	RX		
No shielding	5.24	6.82	426	434	1.66	0.278
Al. shielding	0.83	1.14	90	94	0.02	0.021
Fe. shielding	10.5	13.5	539	595	4.98	0.418
Fe. + Al.	10.0	12.8	534	573	4.39	0.388

Shielding method	Coil-coil max. efficiency	Leakage field 10 mm above RX [μH]	Al. weight [kg]	Fe. weight [kg]
No shielding	98.34%	300	0	0
Al. shielding	37.01%	0.02	0.9	0
Fe. shielding	99.16%	73	0	7.7
Fe. + Al.	99.07%	0.41	0.9	7.7

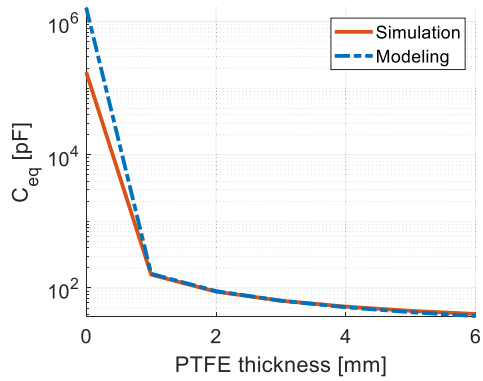

Fig. 5. Equivalent capacitance between two adjacent coil turns.

traditional coils at distances much further than the dielectric thickness [4], the shielded coil performance will degrade under misalignment, in the same manner as two non-SR misaligned coils [21], [22], [23]. The unique SR structure will not give additional design challenges when misaligned.

Based on the case study above, ferrite cores and aluminum plates are needed together for shielding in a complete high-frequency SR coil pad design as shown in Fig. 3(e). Ferrites are used to channel the flux around the coil, increasing the inductance and coupling coefficient, and aluminum plates shield the remaining stray field and also provide mechanical support to mount the coil on the vehicle. Design analysis and optimization are needed to quantify the tradeoff between shielding weight and performance. In the following section, a more detailed analysis is provided, giving shielding design guidelines for optimal power density.

III. SHIELDING DESIGN GUIDELINES CONSIDERING THE PARASITIC CAPACITANCE WITH FERRITES

Compared to conventional 85 kHz EV WPT systems, high-frequency SR coils are more sensitive to parasitic parallel capacitance between winding turns, which needs to be addressed

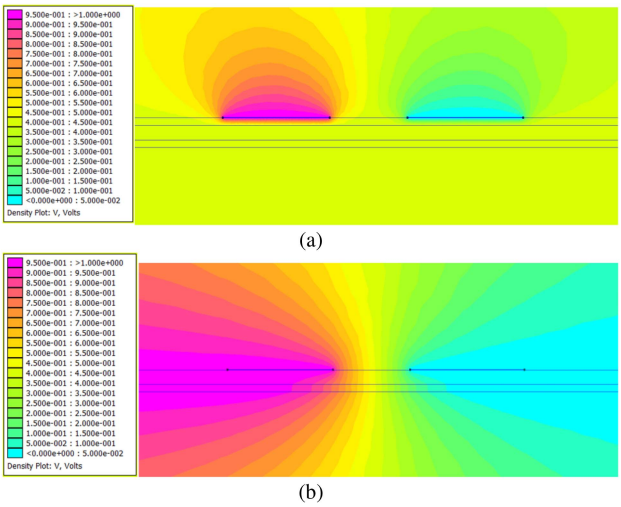

Fig. 6. Electric potential plot comparison. (a) PTFE thickness = 1 mm. (b) No PTFE layer.

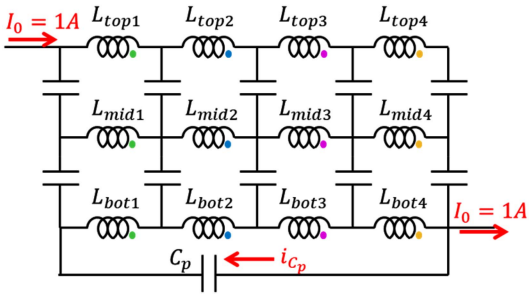

Fig. 7. Lumped element model for three-layer nonuniform SR coil with an equivalent parallel parasitic capacitance.

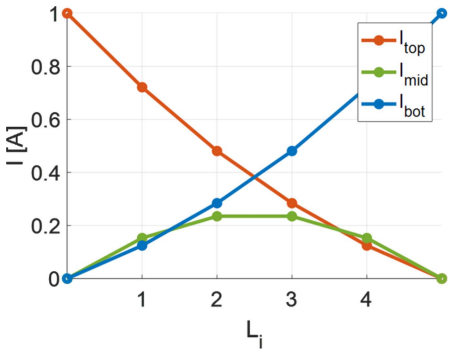

Fig. 8. Current distribution in distributed inductors in the lumped element model when $C_p = 0$.

in the shielding design procedure. There are multiple studies detailing WPT shielding design using ferrites and metal plates, yet no work in the current literature has studied the shielding impact on multi-turn SR coils suitable for EV WPT.

Any SR coil or traditional lumped-capacitance coil exhibits a parasitic parallel capacitance due to the turn-to-turn and turn-to-shield capacitances. In low-frequency, sub-MHz, designs the resonance introduced by this parallel capacitance is often orders of magnitude higher frequency than the series resonant frequency, and minimally impacts operation. For the proposed

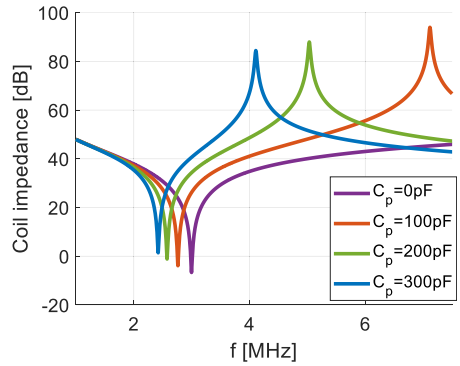

Fig. 9. Coil impedance with varying equivalent capacitance as a function of frequency.

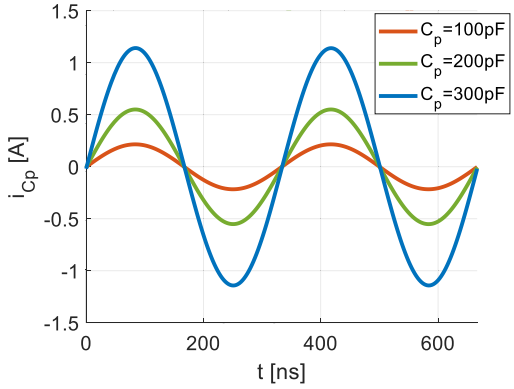

Fig. 10. Parallel capacitance current i_{Cp} with varying equivalent capacitance at 3 MHz.

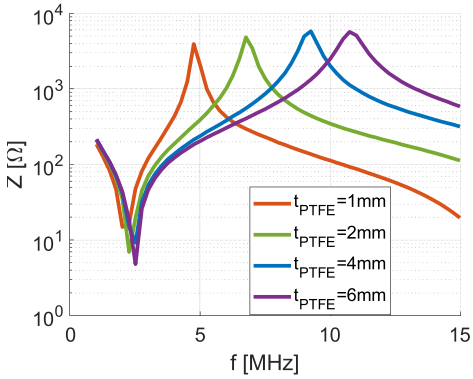

Fig. 11. Coil impedance plot with varying PTFE thickness in HFSS.

high-frequency SR coils, the parallel resonance introduced by the shielding material can be close to the series resonant frequency. Therefore its impact on the coil performance needs to be considered during the design process.

The electric potential is simulated between two adjacent turns of the coil as shown in Fig. 4. Below the coil, a 2 mm thick layer of DMR51W ferrite material [24] and a 1 mm thick aluminum sheet are used for shielding. To tune the parasitic capacitance, the distance between the copper windings and ferrite is varied. For structural support, this spacing is filled with a polytetrafluoroethylene (PTFE), e.g., Teflon, gap-filler. Because the intended purpose of this spacer is purely mechanical, a low-cost, low

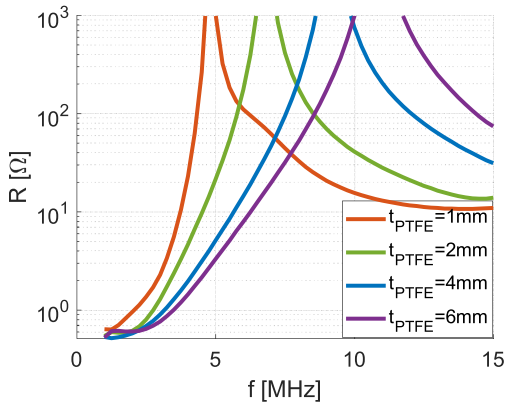

Fig. 12. Coil ESR plot with varying PTFE thickness in HFSS.

TABLE II
RESONANT FREQUENCY AND ESR OF COIL WITH VARYING PTFE THICKNESS

PTFE thickness [mm]	1	2	3	4
Series resonant frequency [MHz]	2.12	2.31	2.40	2.45
Parallel resonant frequency [MHz]	4.89	6.85	9.18	10.82
ESR [Ω]	1.030	0.704	0.657	0.632

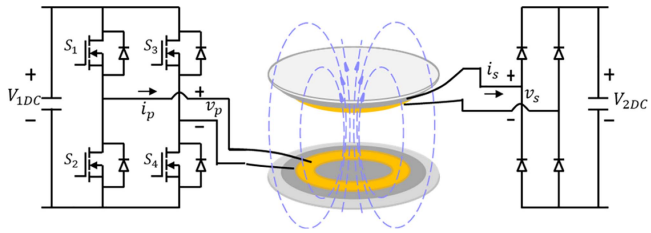

Fig. 13. WPT system circuit diagram with proposed SR coils.

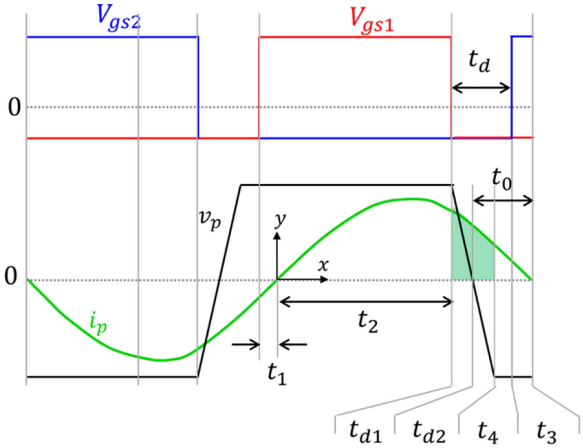

Fig. 14. Waveforms for inverter gate signals V_{gs1}, V_{gs2}, and inverter switching node voltage v_p, current i_p within one switching cycle.

dielectric constant, and low-loss, material is preferred. PTFE is widely available in a variety of thicknesses, has dielectric constant $\varepsilon_r = 2.1$, and has dielectric loss tangent $\tan\delta = 0.0003$.

Between the two adjacent copper traces, there are four parasitic capacitances that are connected in series: C_1 and C_2 formed between the aluminum plate and copper trace on the left, C_3 and C_4 formed between the aluminum plate and copper trace on the right. The total equivalent capacitance is

$$C_{\text{eq}} = \frac{1}{\frac{1}{C_1} + \frac{1}{C_2} + \frac{1}{C_3} + \frac{1}{C_4}}. \tag{1}$$

Each capacitance is calculated using potential-theoretic method based on Fourier series expansion for the electric field [25]

$$\phi\ (x, y) = \sum_{n=1}^{\infty} A_n \sin\left(k_n y\right) e^{-k_n x} \tag{2}$$

where A_n and k_n are constants determined by the boundary conditions for electric potential around the parallel plate.

Note that C_1 and C_4 are much smaller than C_2 and C_3 if the thickness of PTFE and DMR51W are comparable. This is caused by the very high dielectric constant for DMR51W, close to 40 000 (dielectric constant = 38700 @ 3 MHz) [26]. In other words, the total equivalent capacitance is dominated by the capacitance contributed by the PTFE layer.

By varying the PTFE layer thickness, the equivalent capacitance between two coil turns can be tuned accordingly as shown in Fig. 5. If the PTFE layer is too thick, although the value

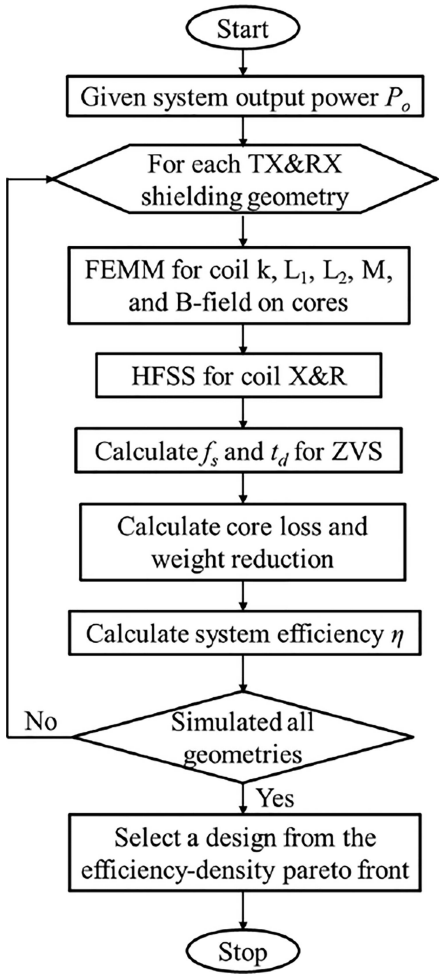

Fig. 15. Design flow chart for shielding optimization.

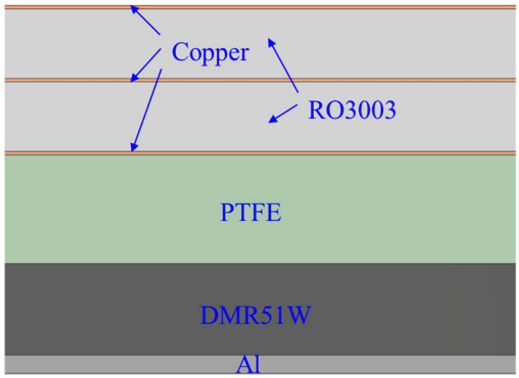

Fig. 16. Cross-section view of shielding structure for optimization with detailed material information.

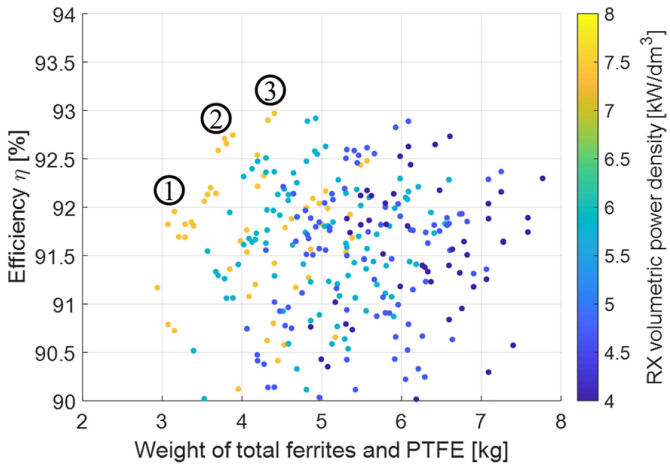

Fig. 17. System optimization result.

TABLE III
DESIGN PARAMETERS ON CASES ON THE PARETO FRONT

No.	η [%]	Fe [kg]	PTFE [kg]	Fe thickness [mm]		PTFE thickness [mm]		Fe inner radius [mm]	
				TX	RX	TX	RX	TX	RX
1	91.95	2.18	0.97	2	2	2	2	75	25
2	92.71	2.27	1.51	2	2	4	2	50	25
3	92.97	2.33	2.08	2	2	6	2	25	25

of the equivalent capacitance can be reduced until the parallel resonance is negligible, the power density of the coil is sacrificed due to the increased weight and size of the PTFE layer.

On the other hand, if the PTFE layer is designed to be too thin, the power density of the coil pad is improved, but there will be high parallel capacitance, leading to a lower parallel resonant frequency and reduced coil performance. Note that when the thickness of the PTFE layer is zero (no PTFE layer exists), the pattern of electric potential changes completely as shown in Fig. 6 due to the conductivity of the ferrites. Accordingly, a minimal electrical insulator is always required between the copper traces and ferrites in the final assembly.

To better understand the impact of the parallel resonance on the coil performance, a lumped element model of a complete three-layer SR coil with the parallel parasitic capacitance

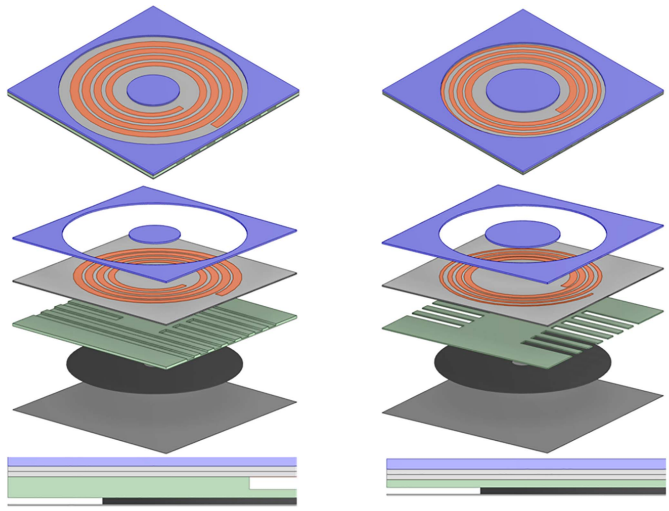

Fig. 18. 3-D exploded and side views of two coil pads. (a) Transmitter coil pad. (b) Receiver coil pad.

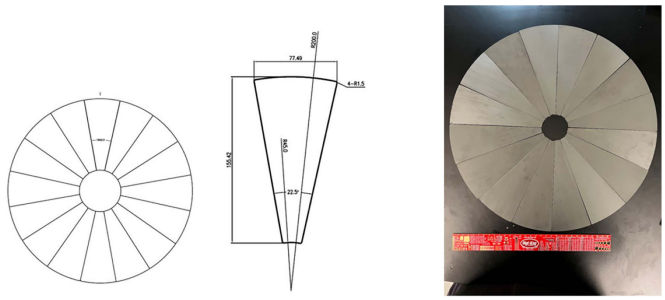

Fig. 19. DMR51W cores. (a) Drawing of fabrication plan. (b) Fabricated ferrite cores.

is shown in Fig. 7. Each copper spiral layer is divided into four segments and approximated by four lumped inductors as an example. Though these impedances are evenly distributed throughout the coil length, the four-segment lumped model is a sufficient approximation to show the varying current flow in each segment of the coil. A series of distributed capacitors are used to model the varying interlayer capacitance along the copper trace due to the varying copper width. Fig. 8 shows the current in each of the lumped inductors. Due to the asymmetric capacitance between any two vertically-connected capacitors, displacement current drives current from the top layer to the bottom layer over the length of the coil [18]. One additional capacitor C_p is used to simulate the impact from PTFE and ferrites; the corresponding coil impedance is shown in Fig. 9.

When shielding is not considered, $C_p = 0$, the three-layer SR coil resonates at 3 MHz as originally designed. With higher parasitic capacitance, the parallel resonant frequency decreases, as shown in Fig. 10. As the parasitic parallel resonance moves closer to the series resonant frequency, the equivalent ESR for the whole coil will increase.

To verify the analysis of the coil model in the lumped element model mentioned above and quantify the impact of the change of

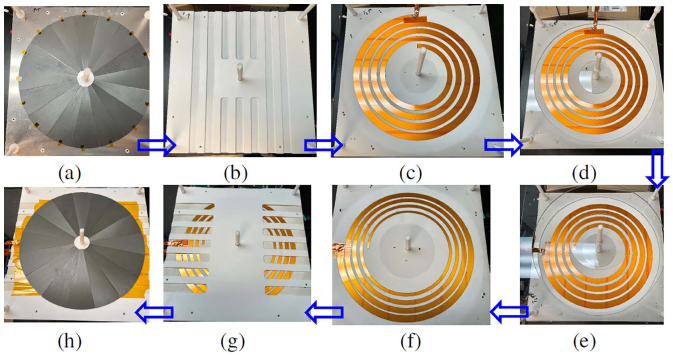

Fig. 20. Shielded coil pad assembly sequence. (a) *TX* Al+Fe. (b) *TX* PTFE spacer. (c) *TX* coil. (d) *TX* polycarbonate clamps. (e) *RX* polycarbonate clamps. (f) *RX* coil. (g) *RX* PTFE spacer. (h) RX Fe+Al.

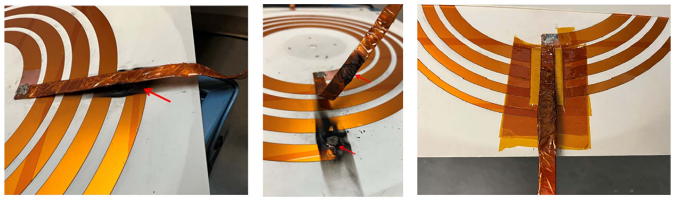

Fig. 21. Insulation treatment. (a) Original design. (b) Insulation breakdown. (c) Updated design.

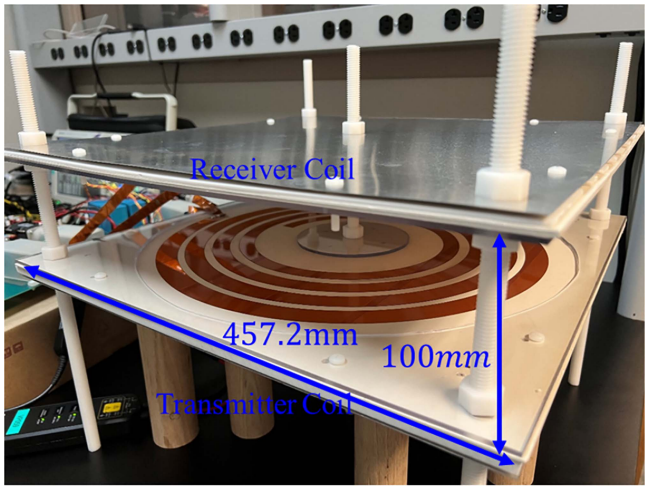

Fig. 22. Complete assembly for coils with shielding.

resonant frequency on the ESR, a 3-D electromagnetic simulation is performed. Figs. 11 and 12 give the high-frequency structure simulator (HFSS) simulation results of the coil impedance and ESR, respectively, with varying PTFE thickness over a frequency range from 1 to 15 MHz in 250 kHz steps. The original coil without shielding has 5 μH inductance and 3 MHz resonant frequency.

With the increasing PTFE thickness, the parasitic capacitance caused by the shielding continues to decrease, leading to a higher parallel resonant frequency and lower coil ESR, which verifies the analysis of the lumped element model. The simulation results with different PTFE thicknesses are given in Table II. With larger

TABLE IV
SHIELDED COIL PADS BILL OF MATERIALS

Name	Part number	Quantity	Dimension [mm]	Total weight [kg]
		TX coil pad		
Coil ceramics	RO3003	2	457.2x457.2x1.5	1.317
Copper	RO3003	NA	4 turns, 2oz	0.116
Ferrite	DMR51W	16	155.42x77.49	1.163
PTFE	McMaster 8545K46	1	457.2x457.2x6.35	2.247
Aluminum	McMaster 6061	1	457.2x457.2x0.4064	0.229
Polycarbonate	McMaster 8574K53	1	457.2x457.2x3.175	0.309
Total				5.381
		RX coil pad		
Coil ceramics	RO3003	2	457.2x457.2x1.5	1.317
Copper	RO3003	NA	3-layer, 4 turns, 2oz	0.088
Ferrite	DMR51W	16	155.42x77.49	1.163
PTFE	McMaster 8545K46	1	457.2x457.2x2.381	0.856
Aluminum	McMaster 6061	1	457.2x457.2x0.4064	0.229
Polycarbonate	McMaster 8574K53	1	457.2x457.2x3.175	0.450
Total				4.103

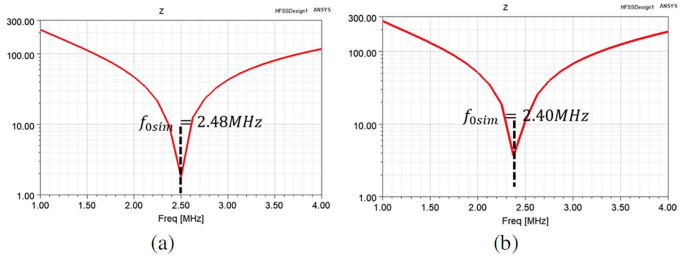

Fig. 23. Impedance results of the shielded coil in HFSS simulation. (a) Transmitter coil. (b) Receiver coil.

TABLE V
SHIELDED SR COILS CHARACTERIZATION AND COMPARISON

	HFSS simulation (core loss not included)	Impedance analyzer
	TX coil pad	
f_0 [MHz]	2.48	2.42
L [µH]	7.26	7.72
C [pF]	567.8	562.9
R [Ω]	0.593	0.639
	RX coil pad	
f_0 [MHz]	2.40	2.42
L [µH]	10.12	9.84
C [pF]	435.6	438.8
R [Ω]	0.957	0.878
	Two coil pads	
k	0.278 (FEMM)	0.272

parasitic capacitance, both coil quality factor and series resonant frequency are decreased.

To quantitatively evaluate the shielding impact on the coil quality factor, and to facilitate the best tradeoff between the electrical performance and the power density, the shielding structure is optimized together with the system design in the following section.

IV. SYSTEMATIC SHIELDING GEOMETRY OPTIMIZATION

Since the shielding design will strongly impact the tradeoff between system efficiency and power density, a system-level design optimization procedure is proposed to optimize the shielding geometry. The inverter and rectifier are modeled and designed in [18], with GaN systems GS66516T 650 V GaN transistors and CREE C4D08120E 1200 V SiC Schottky diodes

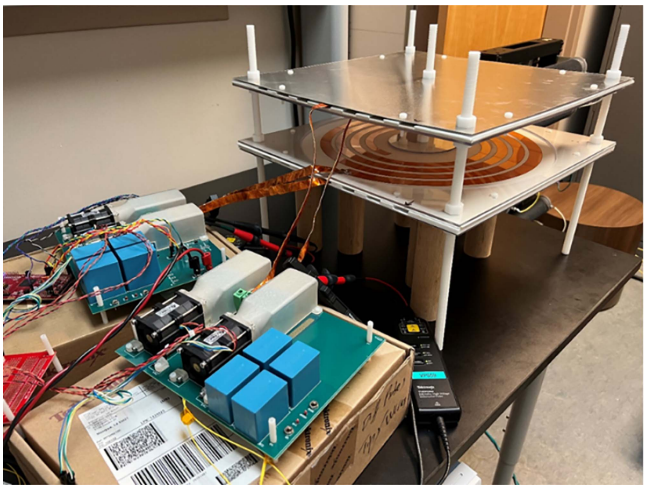

Fig. 24. WPT system with shielded SR coils.

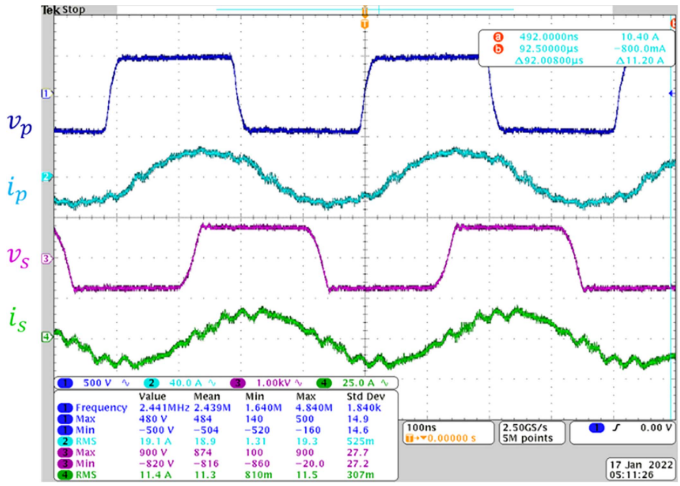

Fig. 25. 6.6 kW system power test waveforms.

implementing the high-frequency inverter and rectifier, respectively. The system circuit diagram is shown in Fig. 13.

Zero-voltage-switching (ZVS) of the inverter is guaranteed by tuning the switching frequency f_s around the coil resonant frequency f_0 with the shielding impact considered. As shown in Fig. 14, a slightly positive phase shift is needed between the switching node voltage v_p and current i_p to allow enough charge, $2Q_{\text{oss}}$, to complete the ZVS process of one phase leg.

For the completion of ZVS, time intervals t_{d1} and t_{d2} need to fulfill

$$Q_{\text{oss}} = \int_{\frac{T_s}{2}-t_0-t_{d1}}^{\frac{T_s}{2}-t_0} \sqrt{2} I_p \sin(\omega_s t) dt \tag{3}$$

$$Q_{\text{oss}} = \int_{\frac{T_s}{2}-t_0}^{\frac{T_s}{2}-t_0+t_{d2}} \sqrt{2} I_p \sin(\omega_s t) dt \tag{4}$$

where I_p is the RMS value of i_p, and the switching dead time t_d is selected such that

$$t_{d1} + t_{d2} \le t_d \le t_{d1} + t_0. \tag{5}$$

TABLE VI
SYSTEM TESTED RESULT COMPARISON

	Input voltage [V]	Transmitter current I_p [A]	Load voltage V_{2DC} [V]	Receiver current I_s [A]	Efficiency η
Model	494.7	17.8	726.6	11.5	93.1%
Test	471.8	19.1	733.6	11.4	92.3%

TABLE VII
SYSTEM TESTED EFFICIENCY AT DIFFERENT LOAD

Power [kW]	1	2	3	4	5	6.6
Input voltage [V]	190	264	321	369	411	472
Transmitter current I_p [A]	7.4	10.4	12.8	14.7	16.5	19.1
Load voltage V_{2DC} [V]	285	403	494	571	639	734
Receiver current I_s [A]	4.5	6.3	7.7	8.7	9.8	11.4
Efficiency [%]	93.0	92.9	93.0	93.0	92.6	92.3

The system design flow chart for shielding optimization is summarized in Fig. 15, with design iteration on the possible shielding geometry for optimal system efficiency, including ferrite thickness, PTFE thickness, and ferrite disc inner radius. To relieve the calculation burden from 3-D electromagnetic simulation, faster 2-D FEMM-based simulation is first used to calculate the inductance and coupling coefficient of the coils under the influence of the shielding, while 3-D HFSS-based electromagnetic simulation is used to calculate the coil ESR considering the impact from the parallel parasitic capacitance and the dielectric loss from ferrites, which cannot be found by 2-D FEMM magnetostatic simulation. The core loss of the ferrites is estimated by the magnetic field distribution captured from FEMM simulation and core loss data from the datasheet provided by the vendor [24]. Together with the WPT system model proposed in [18], the highest system efficiency is calculated for each shielding geometry.

Parameters including ferrite thickness [2 mm, 4 mm], ferrite disc inner radius [25 mm, 50 mm, 75 mm], and PTFE thickness [2 mm, 4 mm, 6 mm] are swept, and the corresponding HFSS simulation results are incorporated into the WPT system model to calculate the system efficiency, weight of shielding materials, and shielded coil volumetric power density. The dimension of the aluminum plate is 18" $\times$ 18" with 0.016" thickness. The outer radius of the ferrite plate is selected to be the same as the coil pad, 200 mm, to channel the flux from all coil traces. The complete coil and shielding stackup is shown in Fig. 16, with RO3003 as the dielectric for the series resonant capacitance and PTFE as the low-loss spacer used to limit the parasitic parallel capacitance.

Totally 324 cases of shielding design are simulated and optimized. Fig. 17 gives the resulting design performance, as characterized by system efficiency, the total weight of ferrites and PTFE for two coils, and volumetric power density based on the *RX* coil volume, including copper, RO3003 laminates, ferrites, and PTFE spacer. The detailed specifications of three cases on the Pareto front are summarized in Table III. Case no. 3 is selected for the prototype build considering the balance between efficiency, power density, and the cost of magnetic

TABLE VIII
STATE-OF-THE-ART WPT SYSTEM COMPARISON WITH SHIELDING

Institute	Year	Shielding	f [kHz]	DC-DC efficiency	Power [kW]	L [μH] pri./sec.	C [nF] pri./sec.	Relative air gap, $d/\sqrt{A}$	Compensation type	Gravimetric power density [kW/kg]†		Volumetric power density [kW/dm³]†	
										TX	RX	TX	RX
WiTricity [27]	2011	Fe+Al	145	90-93% (AC-DC)	3.3	--	--	0.38	--	0.26‡	0.26‡	0.35‡	0.35‡
ETH [28]	2016	Fe+Cu	85	95.8%	50	71.6/71.6	54.1/54.1	0.29	Series L-C	2.0‡	2.0‡	2.7‡	2.7‡
UA [9]	2019	Fe+Al+Cu	100	92.1% (TX-DC)	7	197/198	--	0.28	Series L-C	--	--	2.4	2.4
UOA [29]	2019	Fe+Al	85	91.2%	5.7	67.5/4.11	--	0.37	Parallel L-C	0.24	1.0	0.62	3.6
UOA [29]	2019	Winding	85	89%	5.7	22.2/4.06	--	0.28	Parallel L-C	0.41	1.0	0.32	3.6
UOA [30]	2021	Fe+Winding	85	91%	4.7	43.2/4.08	--	0.37	Parallel L-C	0.36	0.82	0.29	3.0
NCEPU [10]	2022	Fe+Al	85	95% (coil-coil)	3	415/427	8.45/8.21	0.29	Series L-C	--	--	0.20	0.20
This Work	2022	Fe+Al	2439	92.3%	6.6	7.7/9.8	0.56/0.44	0.28	Self-resonance§	3.2	3.2	4.6	7.1

† Power densities are calculated based on the weight and volume of coil windings and ferrites
‡ Final assembly of coil pad with all passive components are included for weight and volume calculation
§ No lumped compensation capacitor is needed in the prototype

material. Both the transmitter and receiver coils use 2 mm thick DMR51W ferrite with 25 mm inner radius and 200 mm outer radius. The transmitter is implemented with a 6 mm thick PTFE space; the receiver PTFE spacer is just 2 mm thick.

The final 3-D structure of two coil pads is shown in Fig. 18 together with the exploded view and side view. Each material in the stackup is labeled in Fig. 16; additional polycarbonate boards (top, blue layer in Fig. 19) are used to hold each assembly against the aluminum back plate. Additional slots are cut in the square-shaped PTFE spacer boards for weight reduction, better airflow around the copper traces, and to provide channels for wire connections to the terminals.

V. SHIELDING HARDWARE ASSEMBLY AND EXPERIMENTAL VERIFICATION

To validate the above design methodology, a complete WPT system with shielded SR coils is fabricated and tested. Based on the manufacturing capabilities of the vendor, 16 pie-shaped ferrite cores are fabricated and assembled to make one complete ferrite plate of a coil as shown in Fig. 19. Each pie-shaped core has 22.5° center angle with approximately 155.42 mm length.

Fig. 20 gives the assembly process for the shielded coil pads for the test setup. Nylon screws are used to secure the coil pad firmly from the Al plate to the polycarbonate cover plate, with ferrite cores, coil, and PTFE spacer sandwiched between them.

For each coil, one lead wire connects to the innermost turn and passes above the outermost turn, as shown in Fig. 21(a). During testing, arcing occured due to the high voltage between the lead wire connected to the innermost turn and the sharp corner on the outermost turn, even when insulated with one layer of Kapton tape rated at 7 kV. To remedy the situation, multiple layers of Kapton tape are applied together with 0.5 mm thickness thermal pad in Fig. 21(c) to leave enough clearance at the weak point. Fig. 22 gives the final complete assembly for coils with shielding, with 100 mm airgap between two coil pads.

Including the PTFE spacer, the thickness of the transmitter and receiver coil pads are only 11.4 and 7.4 mm, respectively. The complete bill of materials for the coil pad assemblies is given in Table IV, including the aluminum back plate and polycarbonate plate for clamping. The major weight contributor is the PTFE spacer; only 1.2 kg of ferrite is used in each coil. With smaller PTFE thickness on the receiver side, the weight of the receiver coil pad is 20% lighter than the transmitter side.

The impedances of the shielded coils are plotted in Fig. 23, and the corresponding characterization results are given in Table V. Due to the existence of the ferrites, the coil inductance has increased by about 30% compared with the original coil without shielding. In addition, compared with the tested result using an impedance analyzer, there is less than 5% error from the simulation results for parameters including series resonant frequency, inductance, capacitance, and coupling coefficient. Core loss is not included in the HFSS simulation and is calculated separately using the vendor's datasheet. Since core loss is nonlinear, measured coil ESR under small signal bias using an impedance analyzer is only used for fast characterization of the magnetic material, which gives relatively large error compared to the HFSS simulation result.

The hardware setup for the system is shown in Fig. 24, with 6.6 kW power test result shown in Fig. 25. At 2.439 MHz switching frequency, 40 ns deadtime, and 80 Ω load resistor, the system is tested up to 6.6 kW, with 92.3% dc–dc efficiency. The detailed tested parameter comparison in Table VI confirms the validity of the optimization process in the previous section. The measured system efficiency is also detailed in Table VII at different load conditions. The system efficiency at 6.6 kW drops from 95.2% without shielding [18] to 92.3% with shielding, including the aluminum backplane, matching closely to the model prediction in Fig. 17.

Table VIII compares the prototype to other state-of-the-art WPT systems in the literature, considering only comparably-rated designs from publications which also detail the design of a complete shielding solution with greater than 1 kW power delivery. Compared to other systems, the proposed WPT system with SR coils achieves much higher power density at 3.2 kW/kg and 7.1 kW/dm^3 based on the weight and volume of coil windings and ferrites. The power density drops to 2.6 kW/kg when the weight of PTFE is included. Because the

PTFE acts only as a mechanical spacer it can be replaced with an alternate lightweight support material. Even with the mechanical components including the aluminum back plate and polycarbonate clamp considered, the final power densities based on the complete receiver coil pad still reach 1.61 kW/kg and 4.8 kW/dm^3.

VI. Conclusion

This article provides a complete design solution for a high-frequency 6.6 kW WPT system based on the proposed SR coils with shielding considered. As is commonplace, a combination of magnetic and conductive shielding is used to contain the vertical flux. However, due to the high-frequency operation, parasitic capacitance introduced by the shielding material results in substantial degradation of coil quality factor. The high-frequency parasitic capacitance introduced by the shielding material is modeled in detail and an additional PTFE spacer is used to separate the SR coils from the ferrite and aluminum shielding to limit the parallel capacitance. An optimization is presented to manage the tradeoff between the weight and efficiency of the coils.

Prototype coils are designed and fabricated, based on a Pareto-optimal design point with transmitter and receiver coil thicknesses of only 11.4 and 7.4 mm, respectively. The high frequency, SR coil design together with the optimized geometry including a PTFE spacer allow the coils to be implemented with minimal ferrite while maintaining high efficiency. The complete 6.6 kW, 2.4 MHz WPT system is validated using the fabricated SR coils, achieving 92.3% dc–dc efficiency and 7.1 kW/dm^3 volumetric power density. This article demonstrates the first 6.6 kW high-frequency WPT system for EV charging using compact SR coils at frequencies above 1 MHz including a complete magnetic and conductive shielding implementation.

Future work will examine the application of coils to higher power EV WPT systems. Higher power delivery is fundamentally limited by the coil quality factor, so both the novel coil structure and optimized shielding design are valuable research topics for any future study on higher power WPT systems with SR coils.

References

[1] C. M. de Miranda and S. F. Pichorim, "A self-resonant two-coil wireless power transfer system using open bifilar coils," *IEEE Trans. Circuits Syst. II,Exp. Briefs*, vol. 64, no. 6, pp. 615–619, Jun. 2017.

[2] K. Chen and Z. Zhao, "Analysis of the double-layer printed spiral coil for wireless power transfer," *IEEE J. Emerg. Sel. Topics Power Electron.*, vol. 1, no. 2, pp. 114–121, Jun. 2013.

[3] A. L. F. Stein, P. A. Kyaw, and C. R. Sullivan, "High-Q self-resonant structure for wireless power transfer," in *Proc. IEEE Appl. Power Electron. Conf. Expo.*, 2017, pp. 3723–3729.

[4] J. Li and D. Costinett, "Analysis and design of a series self-resonant coil for wireless power transfer," in *Proc. IEEE Appl. Power Electron. Conf. Expo.*, 2018, pp. 1052–1059.

[5] P. H. McLaughlin, Y. Wu, C. R. Sullivan, and J. T. Stauth, "Modeling and design of planar-spiral merged-LC resonators in a standard CMOS process," in *Proc. IEEE 21st Workshop Control Model. Power Electron.*, 2020, pp. 1–8.

[6] H. C. Son et al., "Self-resonant coil with coaxial-like capacitor for wireless power transfer," in *Proc. Asia-Pac. Microw. Conf.*, 2011, pp. 90–93.

[7] P. A. Kyaw, A. L. F. Stein, and C. R. Sullivan, "High-Q resonator with integrated capacitance for resonant power conversion," in *Proc. IEEE Appl. Power Electron. Conf. Expo.*, 2017, pp. 2519–2526.

[8] R. Qin and D. Costinett, "Multi-layer non-uniform series self-resonant coil for wireless power transfer," in *Proc. IEEE Energy Convers. Congr. Expo.*, 2019, pp. 3333–3339.

[9] M. Mohammad, E. T. Wodajo, S. Choi, and M. E. Elbuluk, "Modeling and design of passive shield to limit EMF emission and to minimize shield loss in unipolar wireless charging system for EV," *IEEE Trans. Power Electron.*, vol. 34, no. 12, pp. 12235–12245, Dec. 2019.

[10] H. Zhao et al., "Shielding optimization of IPT system based on genetic algorithm for efficiency promotion in EV wireless charging applications," *IEEE Trans. Ind. Appl.*, vol. 58, no. 1, pp. 1190–1200, Jan./Feb. 2022.

[11] B. Zhang, R. B. Carlson, V. P. Galigekere, O. C. Onar, and J. L. Pries, "Electromagnetic shielding design for 200 kW stationary wireless charging of light-duty EV," in *Proc. IEEE Energy Convers. Congr. Expo.*, 2020, pp. 5185–5192.

[12] S. Kim, H.-H. Park, J. Kim, J. Kim, and S. Ahn, "Design and analysis of a resonant reactive shield for a wireless power electric vehicle," *IEEE Trans. Microw. Theory Techn.*, vol. 62, no. 4, pp. 1057–1066, Apr. 2014.

[13] S. Y. Choi, B. W. Gu, S. W. Lee, W. Y. Lee, J. Huh, and C. T. Rim, "Generalized active EMF cancel methods for wireless electric vehicles," *IEEE Trans. Power Electron.*, vol. 29, no. 11, pp. 5770–5783, Nov. 2014.

[14] M. Lu and K. D. T. Ngo, "Attenuation of stray magnetic field in inductive power transfer by controlling phases of windings' currents," *IEEE Trans. Magn.*, vol. 53, no. 9, Sep. 2017, Art. no. 8700408.

[15] Hybrid - EV Committee, "Wireless power transfer for light-duty plug-in/electric vehicles and alignment methodology," SAE International, p. 194, 2020, doi: 10.4271/J2954_202010. [Online]. Available: https://www.sae.org/standards/content/j2954_202010

[16] L. Gu, G. Zulauf, A. Stein, P. A. Kyaw, T. Chen, and J. M. R. Davila, "6.78-MHz wireless power transfer with self-resonant coils at 95% DC–DC efficiency," *IEEE Trans. Power Electron.*, vol. 36, no. 3, pp. 2456–2460, Mar. 2021.

[17] R. Qin, J. Li, and D. Costinett, "A high-frequency wireless power transfer system for electric vehicle charging using multi-layer nonuniform self-resonant coil at MHz," in *Proc. IEEE Energy Convers. Congr. Expo.*, 2020, pp. 5487–5494.

[18] R. Qin, J. Li, and D. Costinett, "A 6.6-kW high-frequency wireless power transfer system for electric vehicle charging using multilayer nonuniform self-resonant coil at MHz," *IEEE Trans. Power Electron.*, vol. 37, no. 4, pp. 4842–4856, Apr. 2022.

[19] J. Sun, R. Qin, J. Li, D. J. Costinett, and L. M. Tolbert, "Design of a resonant reactive shielding coil for wireless power transfer system," in *Proc. IEEE Appl. Power Electron. Conf. Expo.*, 2021, pp. 1565–1572.

[20] D. C. Meeker, "Finite element method magnetics," *FEMM*, vol. 4, no. 32, pp. 35–46, 2010.

[21] Z. Luo and X. Wei, "Analysis of square and circular planar spiral coils in wireless power transfer system for electric vehicles," *IEEE Trans. Ind. Electron.*, vol. 65, no. 1, pp. 331–341, Jan. 2018.

[22] M. Mohammad, S. Choi, Z. Islam, S. Kwak, and J. Baek, "Core design and optimization for better misalignment tolerance and higher range of wireless charging of PHEV," *IEEE Trans. Transp. Electrific.*, vol. 3, no. 2, pp. 445–453, Jun. 2017.

[23] W. Zhang, J. C. White, A. M. Abraham, and C. C. Mi, "Loosely coupled transformer structure and interoperability study for EV wireless charging systems," *IEEE Trans. Power Electron.*, vol. 30, no. 11, pp. 6356–6367, Nov. 2015.

[24] "New soft magnetic material introduction," DMEGC, Zhejiang, China, 2019. [Online]. Available: https://www.dmegc.de/file_folder/2019_DMEGC_Soft_Magnetic_material_introduction_English.pdf</bib>

[25] S. García-Moreno and M. Bandala-Sánchez, "Fringing capacitance in sections of circular parallel plates with variable overlapping area," *Electron. Lett.*, vol. 49, no. 11, pp. 712–714, 2013.

[26] A. Nabih, R. Gadelrab, Q. Li, and F. C. Lee, "Dimensional effects of core loss and design considerations for high-frequency magnetics," in *Proc. IEEE Energy Convers. Congr. Expo.*, 2021, pp. 5488–5495.

[27] C. Mi, "High efficiency wireless power transfer for EV charging and other applications," in *Proc. IEEE Energy Convers. Congr. Expo.*, 2017, pp. 1–184.

[28] R. Bosshard and J. W. Kolar, "Multi-objective optimization of 50 kW/85 kHz IPT system for public transport," *IEEE J. Emerg. Sel. Topics Power Electron.*, vol. 4, no. 4, pp. 1370–1382, Dec. 2016.

[29] M. G. S. Pearce, G. A. Covic, and J. T. Boys, "Robust ferrite-less double D topology for roadway IPT applications," *IEEE Trans. Power Electron.*, vol. 34, no. 7, pp. 6062–6075, Jul. 2019.

[30] M. G. S. Pearce, G. A. Covic, and J. T. Boys, "Reduced ferrite double D pad for roadway IPT applications," *IEEE Trans. Power Electron.*, vol. 36, no. 5, pp. 5055–5068, May 2021.